

## Chapter 3

### Refolding Kinetics of DNS(C102)-cyt *c*

\*Adapted from J. G. Lyubovitsky, H. B. Gray, J. R. Winkler, *J. Am. Chem. Soc.*, 124, 5481-5485 (2002)

## INTRODUCTION

The production of functional proteins requires that polypeptides find a unique conformation in a vast space of incorrect folds.<sup>1</sup> The consequences of failure are severe; misfolded proteins are implicated in a rapidly growing list of debilitating illnesses that includes type II diabetes as well as Alzheimer's and Creutzfeldt-Jakob diseases.<sup>2</sup> Partially folded polypeptide structures are key intermediates in both the proper assembly of proteins and the formation of harmful misfolded structures.<sup>3-5</sup> Characterizing the structures, energetics, and dynamics of these transient species is an essential step in understanding their benign and malignant pathways.

Proteins often fold quite rapidly ( $<1$  s), because the energy bias on a funnel-shaped landscape steers unfolded peptides toward native conformations.<sup>6,7</sup> The upper rim of the funnel represents a heterogeneous ensemble of unfolded polypeptides; partially folded conformations appear as local minima on this energy surface; and misfolded structures can be in deep energy wells separate from the native minimum. To map this complex energy landscape, it is necessary to probe structural features of the polypeptide ensemble as it evolves to the native state.

We have examined *D-A* distance distributions (Chapter 2) during the folding of *Saccharomyces cerevisiae* iso-1 cytochrome *c* (cyt *c*), a 108-residue, partially helical, heme protein.<sup>8</sup> In prior work, we have shown that the folding kinetics (corrected for driving force) of iso-1 cyt *c* are comparable to those of the more extensively studied equine protein.<sup>9-13</sup> In the folded protein at neutral pH, an imidazole nitrogen (H18)<sup>13a</sup> and a thioether sulfur (M80) axially ligate the heme iron. The nitrogenous base of an amino acid side chain (pH 7: H26, H33, H39) replaces M80 in the unfolded protein.<sup>14</sup> This misligation retards refolding,

because ligand exchange is required for the peptide to adopt its native conformation.<sup>15,16</sup> For FET kinetics experiments, we derivatized the thiolate sulfur of C102 in yeast cytochrome *c* with a dansyl fluorophore (DNS); the DNS label fluoresces intensely when the protein is unfolded in guanidine hydrochloride (GuHCl) solutions, but is significantly quenched by energy transfer to the heme in the folded conformation.<sup>17</sup>

## MATERIALS AND METHODS

The materials and methods relevant to this chapter are described in the corresponding section of Chapter 2. Those introduced in this chapter are described below.

### Fluorescence Decay Kinetics

Folding kinetics probed by fluorescence intensity measurements were obtained by directing light from HeCd laser ( $\lambda_{\text{ex}} = 325 \text{ nm}$ ) through the sample. The emitted light was collected at  $90^\circ$  with a fiberguide (SPC210N, HOH, NaO40, 44 fibers, 1 m, Fiberguide Industries, Inc.), focused onto a monochromator set at 500 nm and detected by a 9-stage photomultiplier tube.

Fluorescence decay measurements were performed using the third harmonic of a regeneratively amplified, mode-locked Nd:YAG laser (355 nm, 50 ps, 0.5 mJ)<sup>18</sup> for excitation, and a picosecond streak camera (Hamamatsu C5680) for detection. Magic-angle excitation and collection conditions were employed throughout.<sup>19</sup> DNS fluorescence was selected with a long-pass cutoff filter ( $>430 \text{ nm}$ ). The C5680 was used in the analogue mode.

## Refolding kinetics

Protein folding was initiated using a BioLogic SFM-4s stopped-flow mixer. The calculated mixing deadtime was  $\sim 1.1$  ms. To test the mixing efficiency, we added  $[\text{Ru}(\text{bpy})_3]\text{Cl}_2 \cdot 6\text{H}_2\text{O}$  (bpy = 2,2'-bipyridine, Strem, 1mM) to the GuHCl syringe and  $[\text{Ru}(\text{NH}_3)_6]\text{Cl}_3$  (Strem, 56 mM) to the buffer syringe. Luminescence decay measurements (data not shown) revealed uniform quenching of  $\text{Ru}(\text{bpy})_3^{2+}$  luminescence by  $\text{Ru}(\text{NH}_3)_6^{3+}$  immediately (1 ms, 22°C or 1°C) after stopped-flow dilution, confirming that the solutions from the two syringes were completely mixed.

FET kinetics were measured during DNS(C102)-cyt *c* folding by synchronizing the regeneratively amplified picosecond Nd:YAG laser<sup>18</sup> with the stopped-flow mixer and streak camera. A gate and delay generator (Stanford Research Systems, Model DG535) was used to program variable delay times between mixing and laser excitation of DNS. Data from 10 to 20 laser shots ([DNS(C102)-cyt *c*] 10  $\mu\text{M}$ ; 200  $\mu\text{L}$  per stopped flow mixing cycle; one laser shot per mix) provided adequate signal-to-noise levels. For cyt *c* refolding kinetics experiments performed in the presence of imidazole (150 mM, Sigma), both the guanidine and the diluting buffer syringes contained the added heterocycle.

In the fluorescence intensity kinetics measurements, data from 7 stopped-flow shots ([DNS(C102)-cyt *c*] 8  $\mu\text{M}$ ; 200-400  $\mu\text{L}$  per stopped flow mixing cycle) were averaged.

## Data Analysis

FET kinetics were analyzed as described in Chapter 2. Fluorescence intensity measurements were fit to a multiexponential function. To check the agreement between the

fluorescence intensity measurements and FET kinetics the following analysis was performed.

According to a two-state model

$$f_U = \frac{I(t) - I(\infty)}{I(0) - I(\infty)}$$

where  $f_U$  is the fraction of unfolded protein.  $I(t)$  is an integrated intensity for a particular delay time described by

$$I(t) = \int_0^{\infty} D(t', t) dt'$$

where  $t'$  is fluorescence decay time and  $t$  is folding time.  $I(0)$  and  $I(\infty)$  are the integrated intensities for the folded and unfolded protein respectively (steady-state FET kinetics, Chapter 2)

$$I(0) = \int_0^{\infty} F(t') dt'$$

$$I(\infty) = \int_0^{\infty} U(t') dt'$$

To adjust intensity in the fluorescence intensity measurement,  $I(0)$  was calculated for each delay time (hence a corresponding value of  $f_U$ ) according to

$$I(0) = \frac{I(\infty) f_U + I(t) - I(\infty)}{f_U}$$

An average value of  $I(0)$  was used. There is a very good agreement between the fluorescence intensity measurement and FET kinetics (**Figure 3.1**).

## RESULTS

### Refolding Kinetics

The DNS fluorescence intensity kinetics, a measure of the ensemble-averaged extent of folding in DNS(C102)-cyt *c* (**Figure 3.2**), can be deconvoluted into three exponential phases when the refolding is triggered by stopped-flow dilution of GuHCl (1.3 to 0.13 M, pH 7, 22 °C): a fast phase ( $\tau_{\text{fast}} = \sim 170$  ms), an intermediate phase ( $\tau_{\text{int}} = \sim 700$  ms), and a slow phase ( $\tau_{\text{slow}} > 4$  s). In the horse heart cytochrome *c* refolding kinetics,<sup>20</sup> the fast phase (5 – 100 ms) is attributed to formation of partially folded intermediate due to association of N- and C-helices.<sup>21-23</sup> The intermediate phase (0.5 – 1 s) is thought to be due to improper heme-histidine ligation<sup>21,22,24</sup> and the slow phase is due to cis/trans isomerization of prolyl peptide bonds. **Table 3.1** shows dependence of observed lifetimes on final [GuHCl].

The integrated DNS fluorescence provides an indication of the extent of folding, but reveals nothing about the structural heterogeneity of the protein ensemble. Measurements of  $I(t)$  at various times during folding (**Figure 3.3**) provide snapshots of *D-A* distance distributions,  $P(r)$ . Immediately after the folding is triggered ([GuHCl] = 0.13 M, 1 ms), we find that 40% of the protein ensemble has collapsed, producing a population with an average *D-A* distance of  $\sim 27$  Å (**Figure 3.4**). Surprisingly, 60% of the protein remains in extended conformations with *D-A* distances greater than 40 Å. Within 10 ms, the  $P(r)$  distribution develops a component at  $\bar{r} = 25$  Å, a value comparable to that of the folded protein. By 50 ms, the 25-Å component is larger than the 27-Å population, and after 400 ms, the latter fraction has nearly disappeared.

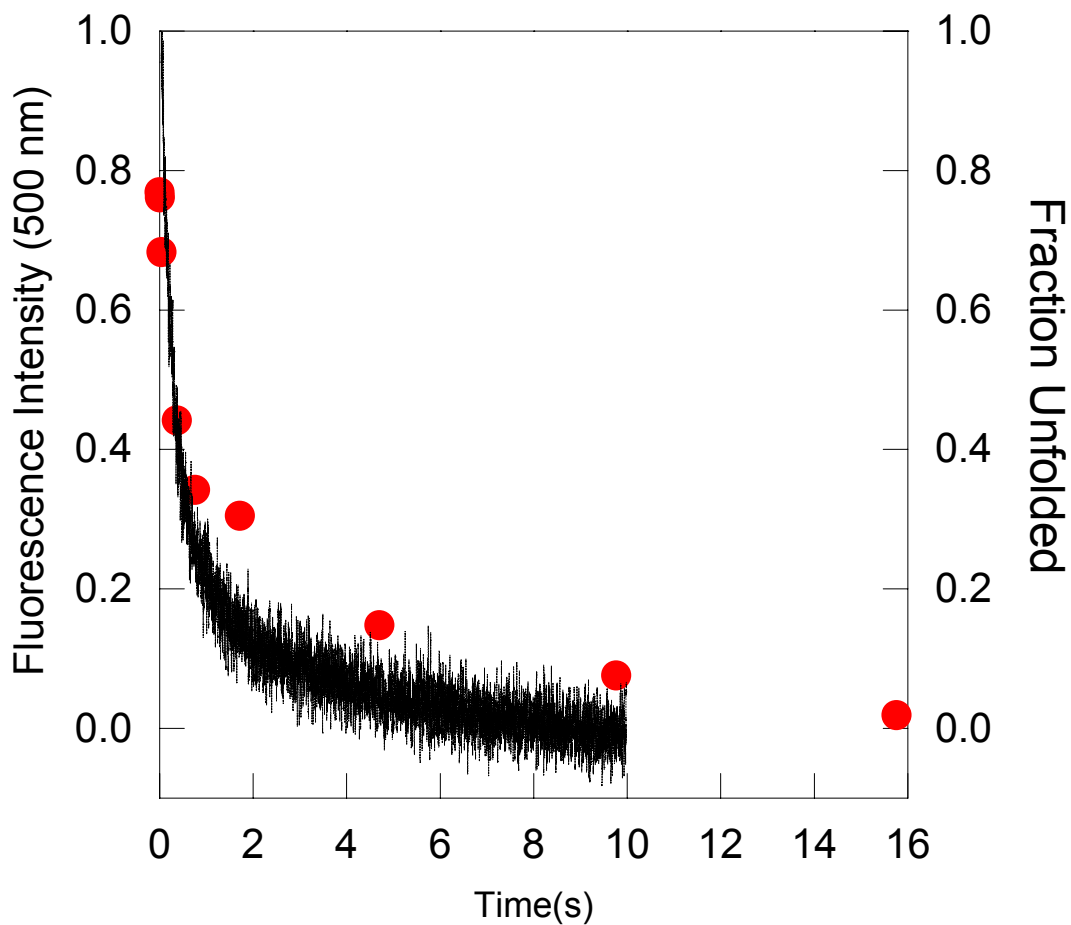


**Figure 3.1.** Time dependence of DNS fluorescence intensity ( $\lambda_{\text{obsd}} = 500 \text{ nm}$ ) during DNS(C102)-cyt c refolding ( $[\text{GuHCl}] = 0.13 \text{ M}$ , pH 7,  $22^\circ\text{C}$ ,  $\lambda_{\text{ex}} = 325 \text{ nm}$ ). Superimposed (circles) are the fractions of unfolded protein from FET kinetics measurements.

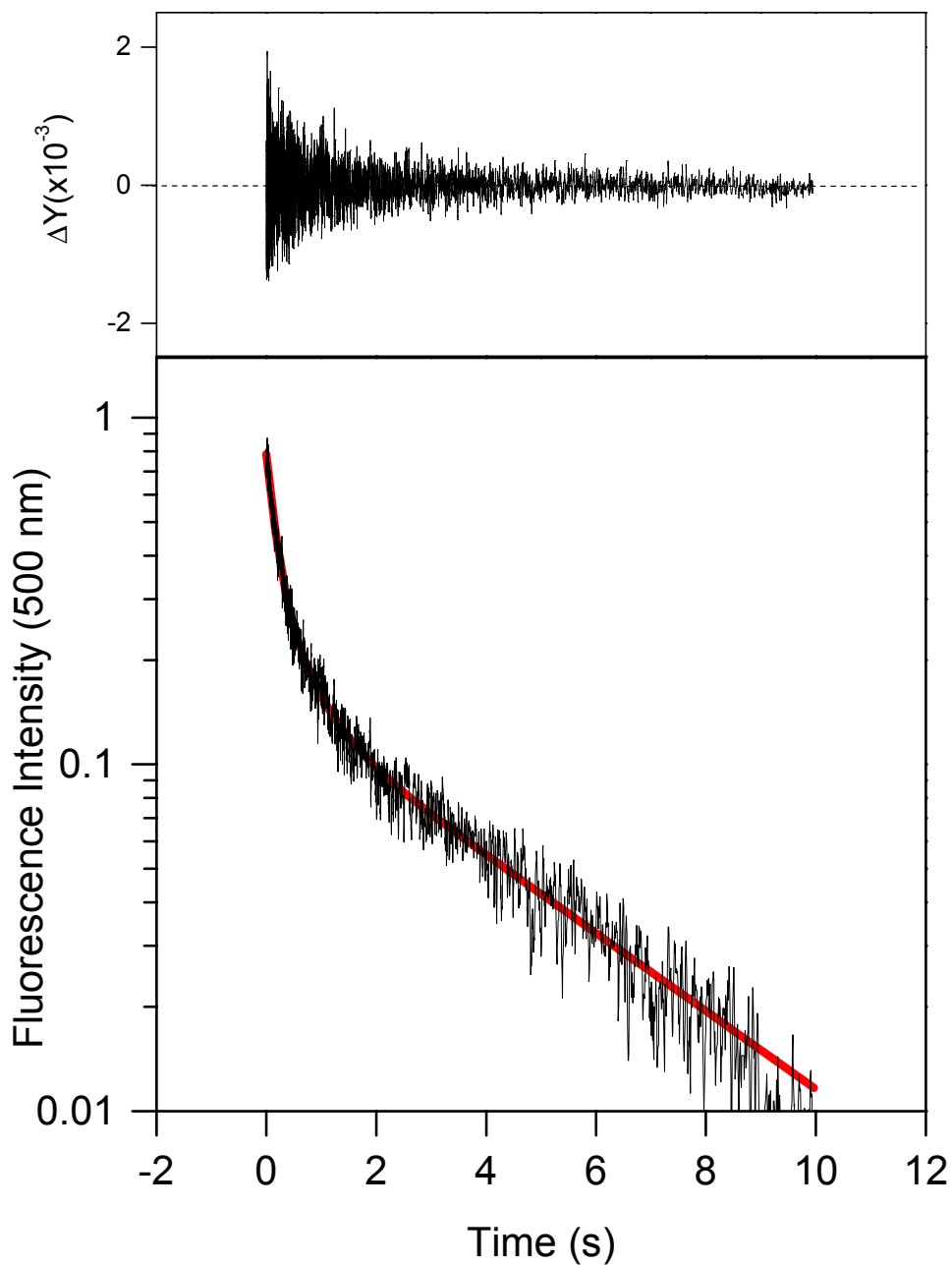


**Figure 3.2.** Time dependence of DNS fluorescence intensity ( $\lambda_{\text{obsd}} = 500 \text{ nm}$ ) during DNS(C102)-cyt *c* refolding ( $[\text{GuHCl}] = 0.13 \text{ M}$ , pH 7,  $22^\circ\text{C}$ ,  $\lambda_{\text{ex}} = 325 \text{ nm}$ ). The smooth line is a fit to an exponential function.

**Table 3.1.** Observed lifetimes and amplitudes for DNS(C102)-cyt c refolding as a function of final [GuHCl]<sup>a</sup>

	$F_1^b$	$\tau_{fast}$ (ms)	$F_2$	$\tau_{int}$ (ms)	$F_3$	$\tau_{slow}$ (s)
[GuHCl] <sub>f</sub> = 0.13 M	0.51	170	0.29	660	0.19	> 4
[GuHCl] <sub>f</sub> = 0.5 M	0.22	230	0.46	690	0.3	> 4
[GuHCl] <sub>f</sub> = 0.8 M	-	-	0.63	590	0.36	> 4

Data were fit using Origin software to the equation:

$$F(t) = F_1 \exp(-t/\tau_{fast}) + F_2 \exp(-t/\tau_{int}) + F_3 \exp(-t/\tau_{slow}) + C$$

where  $F(t)$  is fluorescence intensity as a function of folding time during refolding.  $F_1$ ,  $F_2$ ,  $F_3$ ,  $t_{fast}$ ,  $t_{int}$ ,  $t_{slow}$  are the amplitudes and lifetimes for the observed exponential phases,  $C$  is a constant

<sup>a</sup> Initial [GuHCl] was 1.3 M.

<sup>b</sup> Amplitudes are the fraction of the total observed amplitude.

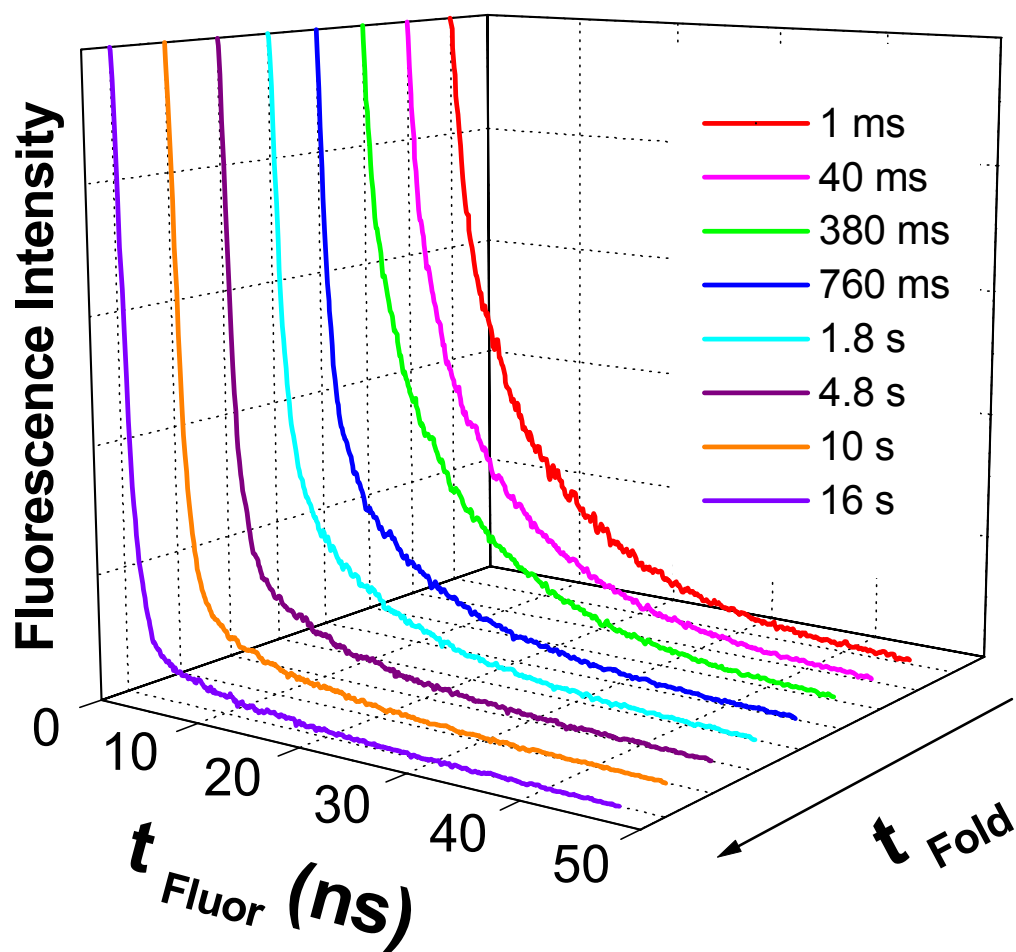


**Figure 3.3.** DNS fluorescence decay kinetics measured at the indicated times after initiation of DNS(C102)-cyt c refolding ( $\lambda_{\text{obsd}} > 434$  nm;  $\lambda_{\text{ex}} = 355$  nm).

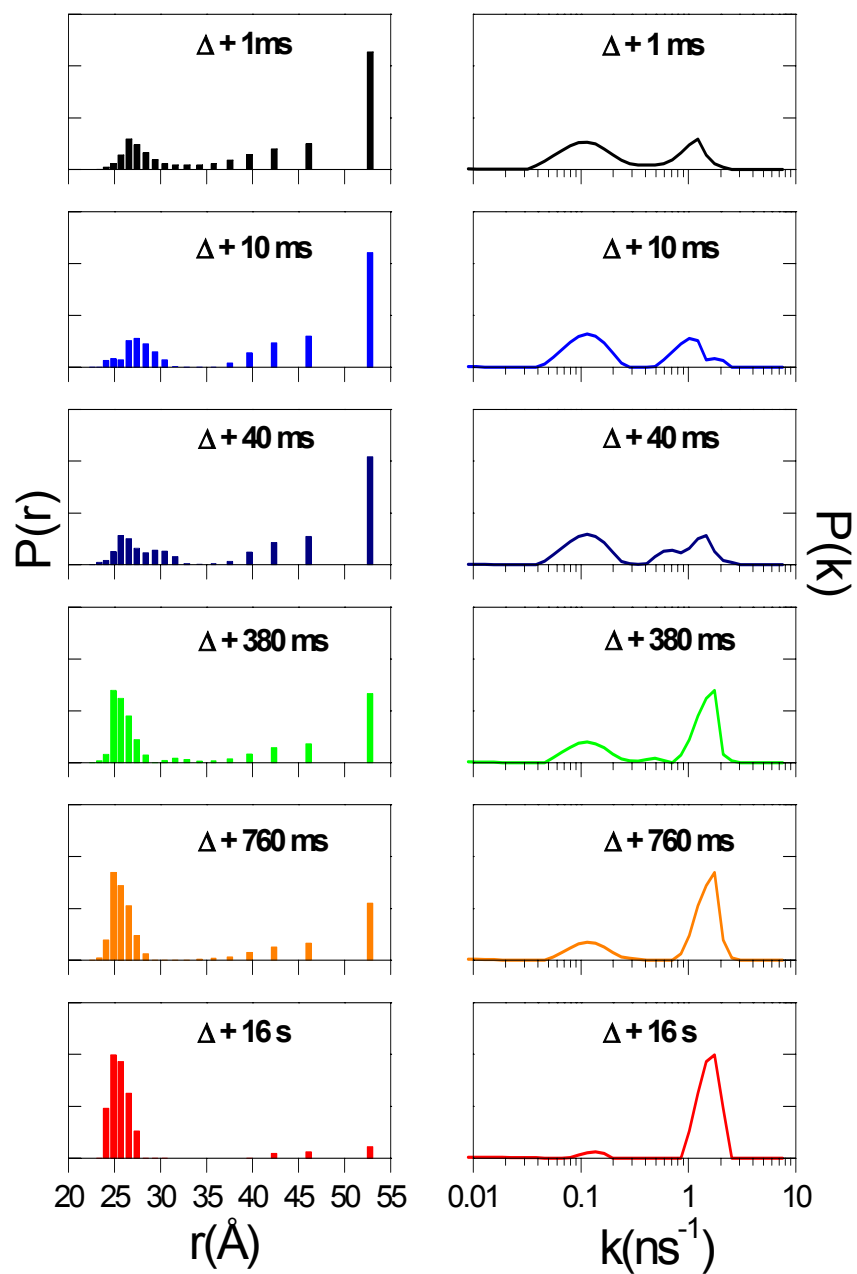


**Figure 3.4.** Evolution of the distributions of luminescence decay rates ( $P(k)$ , right) and  $D$ - $A$  distances ( $P(r)$ , left) in DNS(C102)-cyt  $c$  ( $[\text{GuHCl}] = 0.13 \text{ M}$ ,  $\text{pH } 7$ ,  $22^\circ\text{C}$ ,  $\Delta$  is the mixing deadtime). Kinetics data fit using ME algorithm.

Concomitant with the evolution of the collapsed ensemble, there is a decrease in the population of extended conformations.

It is also interesting to compare how the evolution of the folded ensemble depends on the final [GuHCl]. One millisecond after the folding initiated ([GuHCl] = 0.5 M), we again find that about 40% of the protein ensemble has collapsed, producing a population with an average *D-A* distance of  $\sim 33$  Å (**Figure 3.5**). About 60% of the protein remains in extended conformations with *D-A* distances greater than 40 Å. Only after 180 ms, the  $P(r)$  distribution develops a component at  $\bar{r} = 25$  Å, a value comparable to that of the folded protein. By 760 ms, the 25-Å component is comparable to 33-Å population, and after 5 s, the latter fraction has nearly disappeared. Concomitant with the evolution of the collapsed ensemble, there is a decrease in the population of extended conformations. About 15% of protein ensemble remains unfolded after 16 s of refolding (consistent with the steady-state unfolding, **Figure 2.26, Chapter 2**). If the [GuHCl] is lowered to a midpoint value (0.8 M), we find that early during refolding ([GuHCl] = 0.8 M, 1 ms) only about 25% of the protein ensemble adopts configurations with an average *D-A* distance of  $\sim 33$  Å (**Figure 3.6**). The rest of the protein ensemble exhibits *D-A* distances greater than 40 Å. The  $P(r)$  distribution does not develop a component at  $\bar{r} = 25$  Å, a value comparable to that of the folded protein, until after about 2 s. At 16 s, the amplitude of 25-Å component is comparable to that of 33-Å population and together they account for 50 % of the protein ensemble.

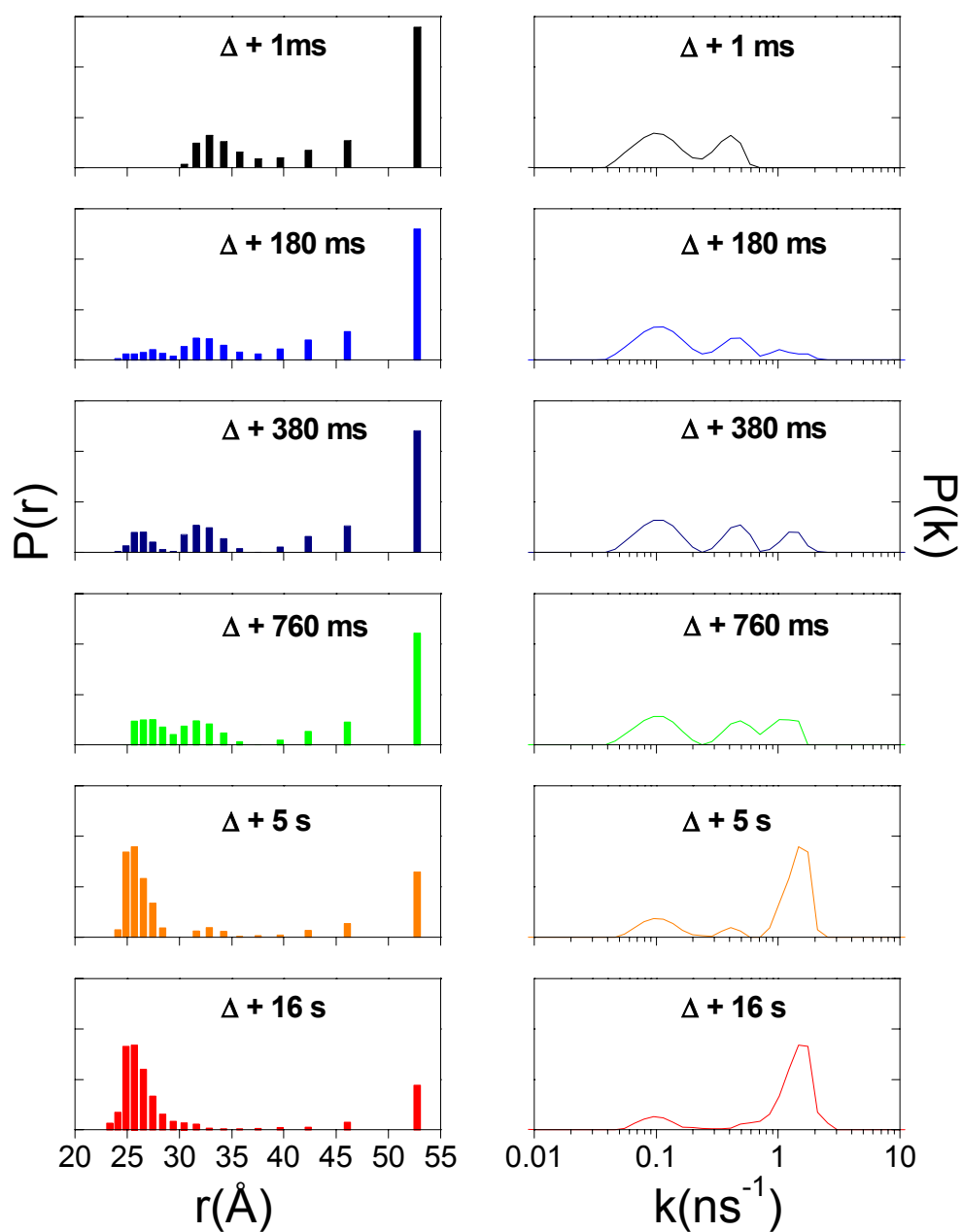


**Figure 3.5.** Evolution of the distributions of luminescence decay rates ( $P(k)$ , right) and  $D-A$  distances ( $P(r)$ , left) in DNS(C102)-cyt  $c$  ( $[\text{GuHCl}] = 0.5 \text{ M}$ ,  $\text{pH } 7$ ,  $22^\circ\text{C}$ ,  $\Delta$  is the mixing deadtime). Kinetics data fit using ME algorithm.

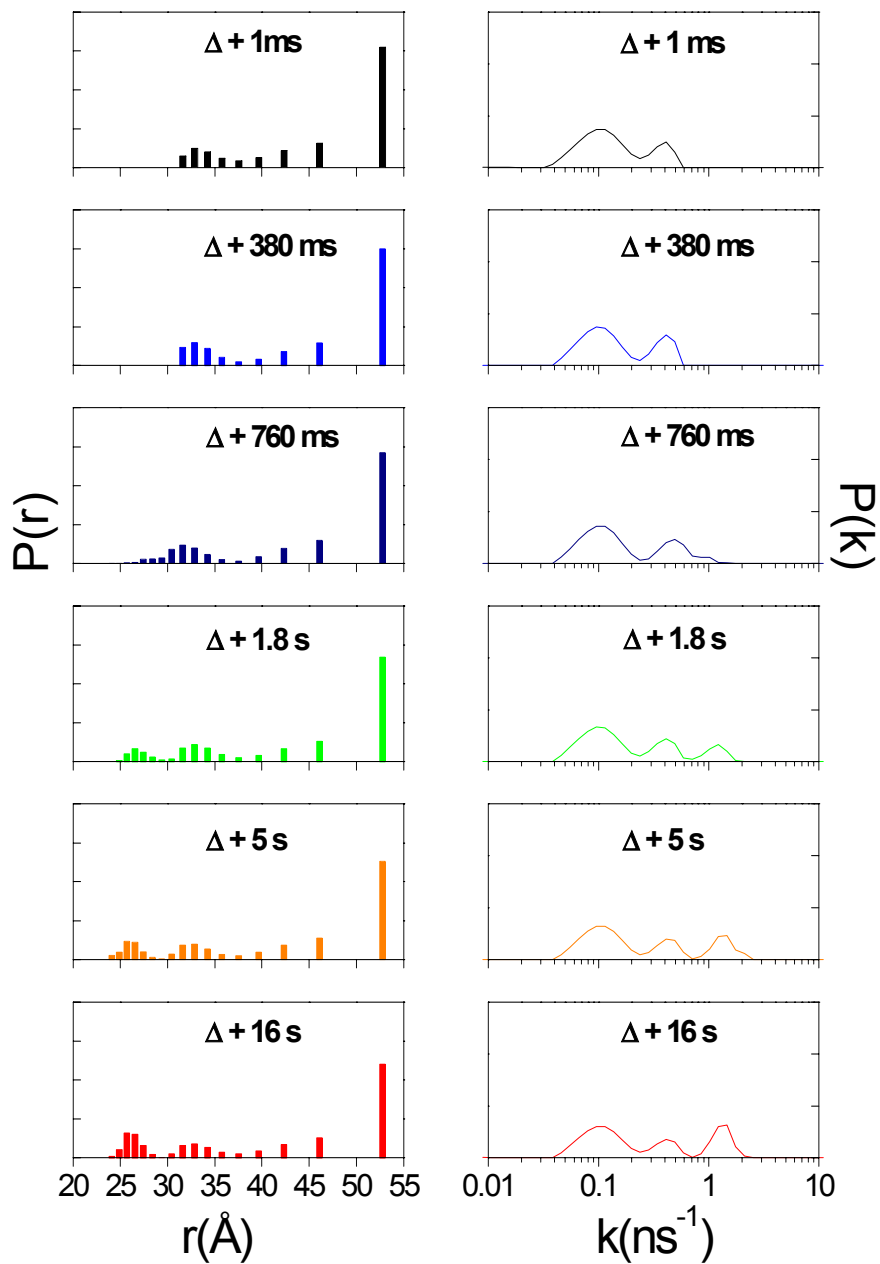


**Figure 3.6.** Evolution of the distributions of luminescence decay rates ( $P(k)$ , right) and  $D-A$  distances ( $P(r)$ , left) in DNS(C102)-cyt *c* ([GuHCl] = 0.8 M, pH 7, 22°C,  $\Delta$  is the mixing deadtime). Kinetics data fit using ME algorithm.

The formation of correctly folded cyt *c* at pH 7 is limited by heme axial ligand substitution processes.<sup>15</sup> Displacement of misligated His groups in denatured cyt *c* by imidazole ([imidazole] = 0.15-0.25 M, [GuHCl] = ~1.8 M, pH 7) dramatically accelerates refolding.<sup>22</sup> NMR investigations of the imidazole adduct of equine cytochrome *c* reveal only modest disruption of the protein structure in the vicinity of the Met80 residue.<sup>25</sup> Measurements of FET kinetics during DNS(C102)-cyt *c* refolding in the presence of imidazole (0.17 M) at room temperature indicate that the native ***D-A*** distance distribution is formed in less than 20 ms. At lower temperature (1 °C), the evolution of ***D-A*** distance distributions (**Figure 3.7**) is remarkably similar to that in the absence of imidazole. The key difference is the overall time scale of refolding; formation of folded protein is largely complete within 200 ms. Roughly equal populations of extended ( $\bar{r} > 50 \text{ \AA}$ ) and collapsed ( $\bar{r} = 32 \text{ \AA}$ ) structures are observed immediately after folding is triggered. The 32-Å distribution evolves into a 25-Å native distribution in ~200 ms.

Substitution of Co(III) in place of iron in DNS(C102)-cyt *c* significantly decelerates refolding.<sup>26,27</sup> The X-ray crystal structure of tuna-Co(III)-cyt *c* showed that the heme environment is not perturbed by the metal substitution.<sup>26,27</sup> The absorption features of Co(III) substituted yeast iso-1 cytochrome *c* are essentially identical to the tuna-Co(III)-cyt *c* and horse-Co(III)-cyt *c* proteins, suggesting similar heme environments.<sup>26,27</sup> The comparison of FET kinetics of DNS(C102)-cyt *c* and DNS-Co(C102)-cyt *c* revealed that similarly structured intermediates are populated in both proteins. The key difference is the timescale: for the Fe(III)-protein, the folded state evolves on the order of milliseconds, Co(III)-protein requires several hours.<sup>27</sup>

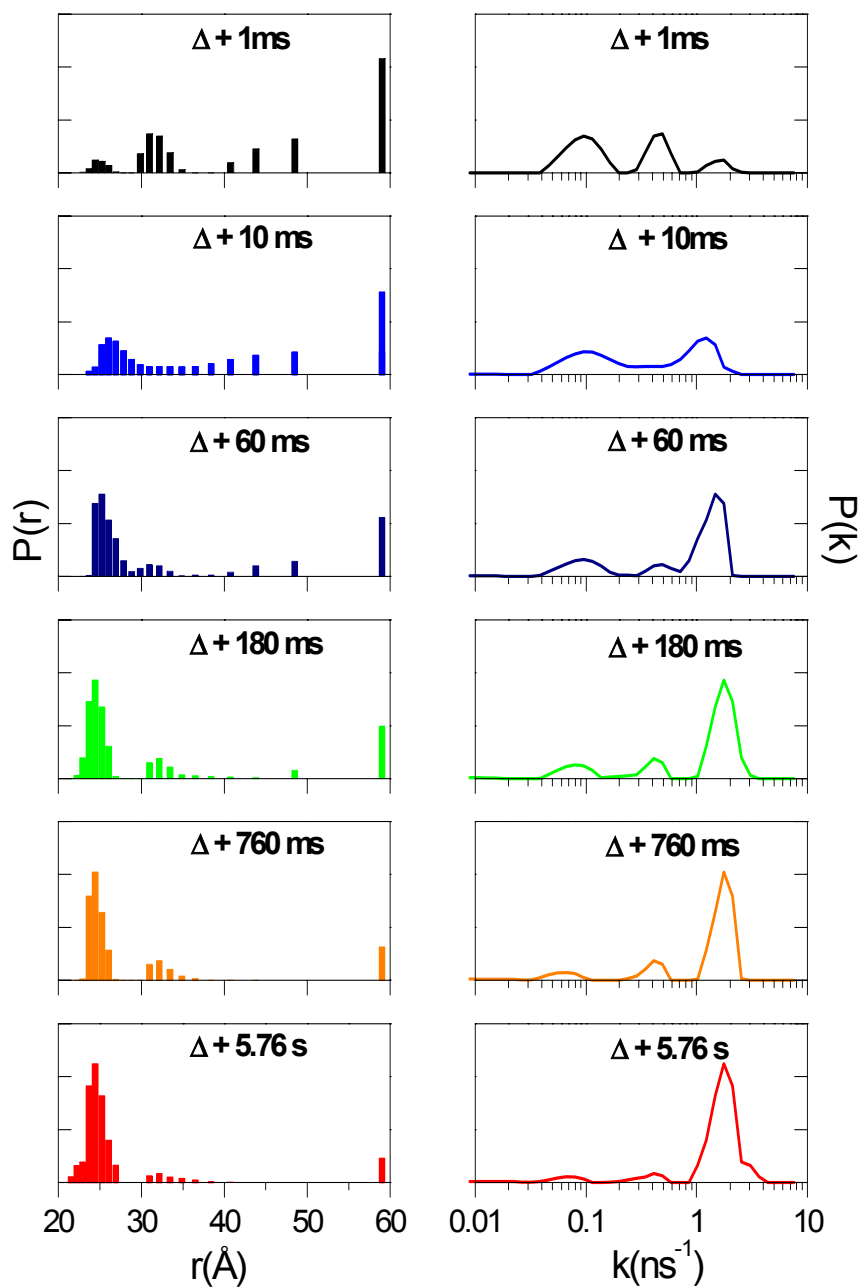


**Figure 3.7.** Evolution of the distributions of luminescence decay rates ( $P(k)$ , right) and  $D-A$  distances ( $P(r)$ , left) in DNS(C102)-cyt *c* ([GuHCl] = 0.13 M, [im] = 0.15 M, pH 7, 1°C,  $\Delta$  is the mixing deadtime). Kinetics data fit using ME algorithm.

## DISCUSSION

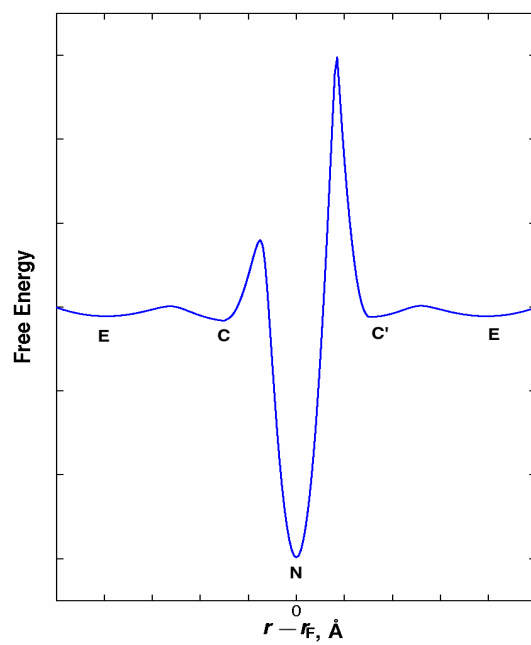
The FET kinetics measured during DNS(C102)-cyt *c* folding indicate that dilution of denaturant to concentrations favoring native protein conformations ([GuHCl] = 0.13 M) does not produce a complete collapse of the polypeptide ensemble. Within the deadtime of stopped-flow measurements, we find that only half of the protein population has formed compact structures. The compact ensemble (**C**) is characterized by a mean DNS-heme separation of  $\sim 27$  Å. This distance is greater than that of the native protein, indicating that the collapsed species are not fully folded.<sup>28</sup> As the population of proteins with the native fold (**N**) increases, the extended (**E**) and compact populations disappear on comparable time scales.

It is surprising that such a large fraction of the protein ensemble remains in an extended conformation after denaturant dilution. These extended conformations are not a consequence of His misligation in the unfolded protein; high concentrations of imidazole displace the His ligands and speed refolding, yet both **E** and **C** fractions are observed at 1 °C. The accelerated cyt *c* refolding in the presence of imidazole also demonstrates that **E** does not arise from kinetically trapped conformations containing proline isomers or incorrect topomers; there is no obvious mechanism by which 150 mM imidazole could eliminate such traps. Indeed, the parallel disappearance of **E** and **C**, rapidly in the presence of imidazole, slowly when His residues misligate the heme and extremely slowly in DNS-Co(C102)-cyt *c*, strongly suggests that the two populations are in rapid equilibrium.<sup>29</sup>

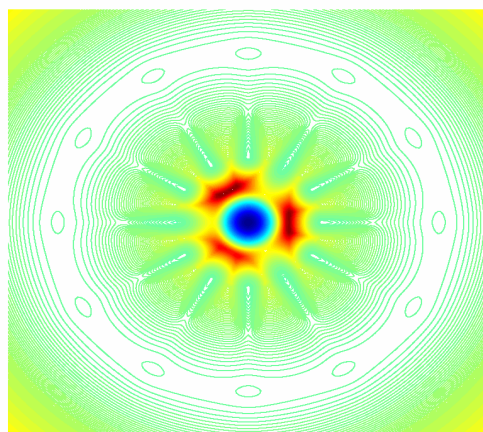
The time-resolved *D-A* distance distributions extracted from FET measurements lead to an *idealized* folding landscape for DNS(C102)-cyt *c* (**Figure 3.8**). The lateral dimension

**Figure 3.8.** Idealized representations of the DNS(C102)-cyt *c* folding landscape. The lateral dimension in all plots is the deviation from the native D-A distance ( $\sim 25$  Å). The two-dimensional cross section of the landscape (a) shows nearly degenerate, shallow energy minima corresponding to extended (**E**) and collapsed (**C**, **C'**) conformations. The collapsed structures on the left side (**C**) of the global energy minimum can surmount a ligand substitution barrier (which can be lowered by the addition of imidazole or raised by  $\text{Co}^{\text{III}}$  substitution) to reach the native (**N**) structure. Collapsed peptides on the right side (**C'**) face a high barrier to formation of the native fold; this population must exchange with other collapsed structures with lower barriers to folding. A contour plot (b) and three-dimensional representation (c) of this idealized folding landscape for DNS(C102)-cyt *c* reveal a flat region on the periphery for extended and compact polypeptides that surrounds the global energy minimum. Some of the compact structures are separated from the native fold by low energy barriers. The remainder have high barriers to native state formation. Polypeptides that fall into these minima must rearrange to extended conformations that can collapse into productive compact structures.

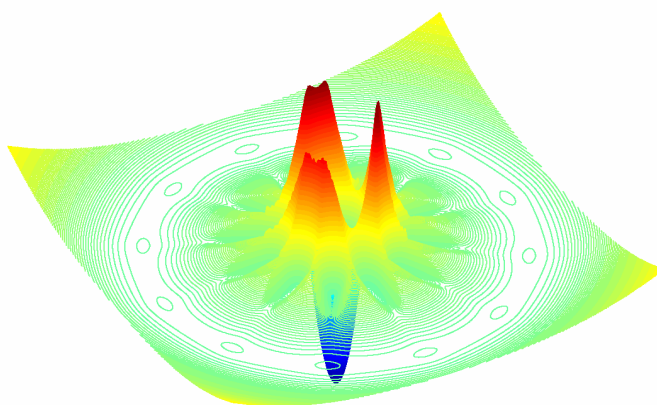
a.



b.



c.



of the landscape is the deviation of the  $D$ - $A$  distance from its value in the folded protein ( $r - r_F$ ;  $r_F \sim 25 \text{ \AA}$ ); and the vertical axis reflects the polypeptide free energy. The cross section of this landscape (**Figure 3.8 a**) illustrates two possible fates for a polypeptide that was in an extended conformation ( $r > 40 \text{ \AA}$ ) prior to the initiation of folding. Denaturant dilution shifts the  $E \rightleftharpoons C$  equilibrium to produce comparable populations of extended and compact polypeptides undergoing rapid exchange ( $\sim 100 \text{ \mu s}$ ). Collapsed conformations (**C**) with favorable arrangements of the polypeptide backbone (topologies) can transform into the native structure (**N**) at pH 7 by surmounting an energy barrier corresponding to a heme axial-ligand substitution process (**Figure 3.8 a**, left path). Rapid collapse of a polypeptide is likely to produce conformations (**C'**) that cannot evolve into the native fold because of backbone-crossing barriers (topological frustration,<sup>30</sup> **Figure 3.8 a**, right path). This model implies that the population of collapsed polypeptides is heterogeneous and that only a fraction of the collapsed conformers are competent to transform into **N**.<sup>30,31</sup> For topologically frustrated compact conformations, the only route to the native state involves formation of an extended polypeptide that can recollapse to a more favorable structure. This mechanism is illustrated by two- and three-dimensional contour plots of the DNS(C102)-cyt *c* folding landscape (**Figure 3.8 b,c**). The native fold is represented by the central free-energy minimum. Owing to the near degeneracy of collapsed and extended polypeptides, the landscape consists of a relatively flat outer rim surrounding a narrow funnel. Rapid interchange among extended conformations via intrachain diffusion proceeds on the outer rim of the landscape.<sup>32-34</sup> These extended polypeptides frequently fall into collapsed conformations toward the interior of the landscape; some of these (3 of the 12 collapsed conformers shown on the idealized surface) can form the native structure; the others must extend and try again. Collapsed and extended

polypeptides in rapid equilibrium at the top of the funnel must wait for a ligand substitution event (pH 7) to open the way to conversion to the native structure at the bottom. Addition of imidazole lowers the ligand substitution barrier and speeds the transformation of collapsed polypeptides into the native form.

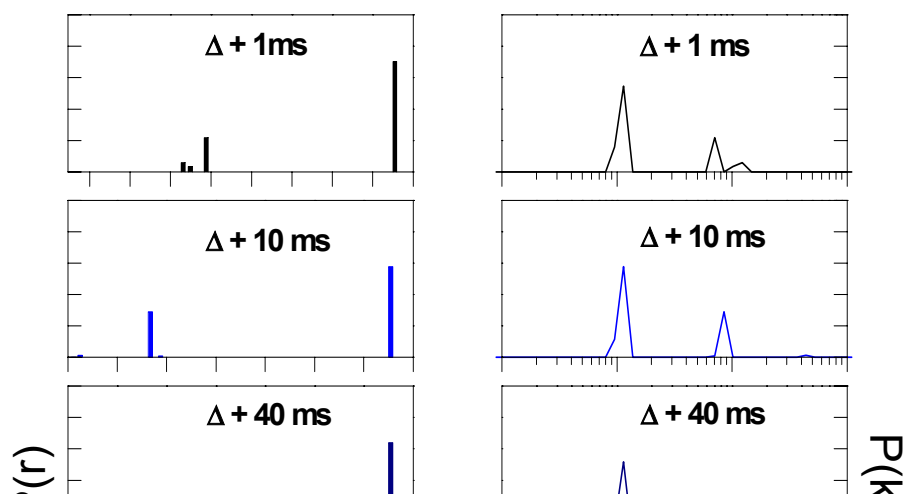
## CONCLUSIONS

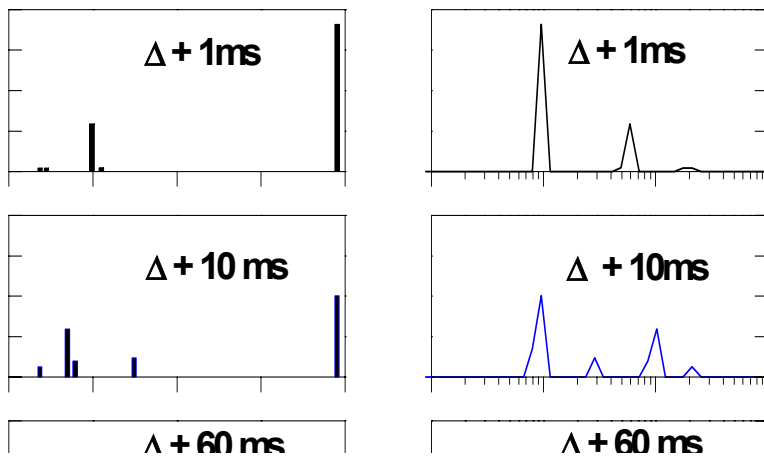
The picture that emerges is one in which extended polypeptide conformations play a pivotal role in DNS(C102)-cyt *c* refolding. Time-resolved FET measurements reveal that, at the onset of folding, fully half of the polypeptide ensemble is found in extended conformations reminiscent of the denatured protein.<sup>28</sup> *The near degeneracy and rapid equilibration of collapsed and extended populations would enable DNS(C102)-cyt c to escape from topologically frustrated compact structures that cannot produce the native fold because of extremely high energy barriers.*<sup>30</sup> If collapsed intermediates were substantially more stable than extended geometries, formation of extended structures would occur infrequently, exacerbating the problem of topological frustration.<sup>30</sup> Instead, DNS(C102)-cyt *c* can collapse and extend many times as it searches for compact structures that have low-barrier routes to the native conformation.<sup>31</sup>

Since collapsed cyt *c* intermediates are not considerably more stable than the fully denatured protein, the likelihood of a native structure rearranging to a partially folded species is substantially lower than would have been the case if collapsed conformations were found in deeper wells on the folding landscape. If this is a common protein folding characteristic, it

may be an important means of avoiding the partially folded intermediates that can aggregate into the misfolded structures that characterize a variety of disease states.

## Supporting Information





**REFERENCES AND NOTES**

- (1) Dill, K. A.; Chan, H. S. *Nat. Struct. Biol.* **1997**, *4*, 10-19.
- (2) Dobson, C. M. *Philos. Trans. R. Soc. B* **2001**, *356*, 133-145.
- (3) King, J.; Haase-Pettingell, C.; Robinson, A. S.; Speed, M.; Mitraki, A. *FASEB Journal* **1996**, *10*, 57-66.

- (4) Nielson, L.; Ritu, K.; Coats, A.; Frokjaer, S.; Brange, J.; Vyas, S.; Uversky, V. N.; Fink, A. L. *Biochemistry* **2001**, *40*, 6036-6046.
- (5) Chiti, F.; Webster, P.; Taddei, N.; Clark, A.; Stefani, M.; Ramponi, G.; Dobson, C. M. *Proc. Natl. Acad. Sci. USA* **1999**, *96*, 3590-3594.
- (6) Bryngelson, J. D.; Onuchic, J. N.; Wolynes, P. G. *PROTEINS: Structure, Function, and Genetics* **1995**, *21*, 167-195.
- (7) Onuchic, J. N.; Lutheyschulen, Z.; Wolynes, P. G. *Annu. Rev. Phys. Chem.* **1997**, *48*, 545-600.
- (8) Scott, R. A.; Mauk, A. G. *Cytochrome c - A Multidisciplinary Approach*; University Science Books: Sausalito, 1996.
- (9) Mines, G. A.; Pascher, T.; Lee, S. C.; Winkler, J. R.; Gray, H. B. *Chem. & Biol.* **1996**, *3*, 491-497.
- (10) Shastry, M. C. R.; Sauder, J. M.; Roder, H. *Acc. Chem. Res.* **1998**, *31*, 717-725.
- (11) Bai, Y.; Sosnick, T.; Mayne, L.; Englander, S. W. *Science* **1995**, *269*, 192-197.
- (12) Yeh, S.-R.; Han, S.; Rousseau, D. L. *Acc. Chem. Res.* **1998**, *31*, 727-736.
- (13) Hagen, S. J.; Eaton, W. A. *J. Mol. Biol.* **2000**, *301*, 1019-1027.
- (13a) the equine cyt c numbering system is used throughout the text
- (14) Colón, W.; P., W. L.; Sherman, F.; H., R. *Biochemistry* **1997**, *36*, 12535-12541.
- (15) Yeh, S.-R.; Takahashi, S.; Fan, B.; Rousseau, D. *Nat. Struct. Biol.* **1997**, *4*, 51-56.

- (16) Telford, J. R.; Tezcan, F. A.; Gray, H. B.; Winkler, J. R. *Biochemistry* **1999**, *38*, 1944-1949.
- (17) Telford, J. R.; Wittung-Stafshede, P.; Gray, H. B.; Winkler, J. R. *Acc. Chem. Res.* **1998**, *31*, 755-763.
- (18) Bachrach, M. *Electron-Transfer in Covalently Coupled Donor-Acceptor Complexes*, Caltech, 1996.
- (19) O'Connor, D. V.; Phillips, D. *Time-correlated single photon counting*; Academic Press:, 1984.
- (20) Colón, W.; Elove, G. A.; Wakem, L. P.; F., S.; Roder, H. *Biochemistry* **1996**, *35*, 5538-5549.
- (21) Elöve, G. A.; Chaffotte, A. F.; Roder, H.; Goldberg, M. E. *Biochemistry* **1992**, *31*, 6876-6883.
- (22) Elöve, G. A.; Bhuyan, A. K.; Roder, H. *Biochemistry* **1994**, *33*, 6925-6935.
- (23) Roder, H.; Elöve, G. A.; Englander, S. W. *Nature* **1988**, *335*, 700-704.
- (24) Sosnick, T. R.; Mayne, L.; Hiller, R.; W., E. S. *Nat. Struct. Biol.* **1994**, *1*, 149-156.
- (25) Banci, L.; Bertini, I.; Liu, G.; Lu, J.; Reddig, T.; Tang, W.; Wu, Y.; Yao, Y.; Zhu, D. *JBIC* **2001**, *6*, 628-637.
- (26) Tezcan, F. A. *Reactions of Heme Proteins in Solutions and Crystals*, California Institute of Technology, 2001.
- (27) Tezcan, F. A.; Findley, W. M.; Crane, B. R.; Ross, S. A.; Lyubovitsky, J. G.; Gray, H. B.; Winkler, J. R. *Proc. Natl. Acad. Sci. USA* **2002**, *99*, 8626-8630.

(28) The mean fluorescence decay rate in the compact intermediate is  $\sim 1.8$  times faster than the decay rate in the folded protein. This small difference in decay rates is found regardless of the fitting method employed (biexponential, LSQNONNEG, ME). Adequate fits to the data cannot be obtained if the decay rate for the compact species is fixed equal to the decay rate for the folded protein. Furthermore, stopped-flow transient absorption measurements on equine cyt *c* demonstrate that M80 coordination to Fe at neutral pH requires several hundred milliseconds (Sosnick, T. R.; Mayne, L.; Hiller, R.; Englander, S. W. *Nature Struct. Biol.* **1994**, *1*, 149-156). It is unlikely, therefore, that the compact structures observed a few milliseconds after denaturant dilution are fully folded.

(29) A  $\sim 100$   $\mu$ s time scale for E  $\leftrightarrow$  C equilibration can be inferred from ultrarapid mixing studies of equine cyt *c* refolding probed by integrated W59 fluorescence. (Shastry, M. C. R.; Sauder, J. M.; Roder, H. *Acc. Chem. Res.* **1998**, *31*, 717-725.; Hagen, S. J.; Eaton, W. A. *J. Mol. Biol.* **2000**, *301*, 1019-1027.)

(30) Thirumalai, D.; Klimov, D. K.; Woodson, S. A. *Theor. Chem. Acc.* **1997**, *96*, 14-22.

(31) Debe, D. A.; Carlson, M. J.; Goddard, W. A. I. *Proc. Natl. Acad. Sci. USA* **1999**, *96*, 2596-2601.

(32) Hagen, S. J.; Hofrichter, J.; Szabo, A.; A., E. W. *Proc. Natl. Acad. Sci. USA* **1996**, *93*, 11615-11617.

(33) Hagen, S. J.; Hofrichter, J.; Eaton, W. A. *J. Phys. Chem.* **1997**, *101*, 2352-2365.

- (34) Lapidus, L. J.; Eaton, W. A.; Hofrichter, J. *Proc. Natl. Acad. Sci. USA* **2000**, *97*, 7220-7225.